

## Ring-shaped polariton lasing in pillar microcavities

V. K. Kalevich,<sup>1,2,a)</sup> M. M. Afanasiev,<sup>1,2</sup> V. A. Lukoshkin,<sup>1,2</sup> K. V. Kavokin,<sup>1,2</sup> S. I. Tsintzos,<sup>3</sup> P. G. Savvidis,<sup>3,4</sup> and A. V. Kavokin<sup>1,5</sup>

<sup>1</sup>*Spin Optics Laboratory, State University of Saint-Petersburg, 1, Ulianovskaya, 198504 St-Petersburg, Russia*

<sup>2</sup>*A.F. Ioffe Physico-Technical Institute, Russian Academy of Sciences, 26, Politechnicheskaya, 194021 St-Petersburg, Russia*

<sup>3</sup>*IESL-FORTH, P.O. Box 1527, 71110 Heraklion, Crete, Greece*

<sup>4</sup>*Department of Materials Science and Technology, University of Crete, 71003 Heraklion, Crete, Greece*

<sup>5</sup>*Physics and Astronomy School, University of Southampton, Highfield, Southampton SO171BJ, United Kingdom*

(Received 20 December 2013; accepted 22 February 2014; published online 5 March 2014)

Optically generated exciton-polaritons in cylindric semiconductor pillar microcavity with embedded GaAs/AlGaAs quantum wells demonstrate a clear polariton lasing regime. When exciting in the center of the pillar, we detect a ring-shaped emission, where the peak of intensity can be separated from the excitation spot by more than 10  $\mu\text{m}$ . The spatial coherence of the ring emission is verified by interferometry measurements. These observations are interpreted by drift of the exciton polariton condensate away from the excitation spot due to its repulsion from the exciton reservoir and by its spatial confinement by the pillar boundary. © 2014 AIP Publishing LLC. [<http://dx.doi.org/10.1063/1.4867519>]

### I. INTRODUCTION

Polariton lasers are devices capable of emitting spontaneously a coherent and monochromatic light.<sup>1</sup> They are based on condensation of mixed light-matter quasiparticles—exciton-polaritons—in a single quantum state in a semiconductor microcavity due to their bosonic nature. Polariton lasers with optical<sup>2</sup> and electrical injection<sup>3,4</sup> have been realized in planar and pillar<sup>5,6</sup> microcavities based on various semiconductor materials.

Exciton-polaritons repel each other due to their excitonic component.<sup>7–9</sup> In the case of optical excitation of a planar microcavity by a sharply focused light beam, this leads to radial drift of polaritons<sup>10,11</sup> and formation of a polariton condensate at some distance from the excitation spot, unlimitedly expanding farther away.<sup>12</sup> The lateral confinement of polaritons in micropillars<sup>13</sup> or microwires<sup>14</sup> helps shaping polariton condensates and may lead to their patterning, which would affect the beam-shape of the emitted light. As an example, in square pillars the emission is located at corners.<sup>13</sup>

Here, we report formation of ring-shaped exciton-polariton condensates in cylindric GaAs/AlGaAs pillar microcavities under nonresonant optical pumping in the center of the pillar by a sharply focused continuous-wave (cw) laser. We have discovered a ring-shaped pattern of spatially coherent emission. The diameter of the emitting ring strongly exceeds the diameter of the excitation spot (2  $\mu\text{m}$ ). It can be as large as 30  $\mu\text{m}$  in the pillar of 40  $\mu\text{m}$  diameter.

Changing the intensity of non-resonant optical excitation, we clearly observe a threshold to polariton lasing, which is manifested by the increase of the intensity of emission by several orders of magnitude and by significant narrowing of the emission line. The distribution of polaritons in the reciprocal space develops a sharp peak near  $k=0$ . The

spatial coherence builds up, which is evidenced by interferometry measurements. All these findings confirm the onset of a polariton lasing regime with a peculiar ring-shaped pattern of emission.

### II. EXPERIMENTAL

We studied the set of cylindric pillars, which were produced by etching the MBE-grown planar  $5\lambda/2$   $\text{Al}_{0.3}\text{Ga}_{0.7}\text{As}$  microcavity with top and bottom distributed Bragg reflectors (DBRs) consisting of 32 and 35 pairs of  $\text{AlAs}/\text{Al}_{0.15}\text{Ga}_{0.85}\text{As}$ , respectively, and having the quality factor  $Q > 16000$ . Four sets of three 10 nm  $\text{Al}_{0.3}\text{Ga}_{0.7}\text{As}/\text{GaAs}$  quantum wells (QWs) are placed at antinodes of the cavity electric field in order to maximize the exciton-photon coupling strength.<sup>15</sup> A wedge in the cavity thickness permits variation of the detuning energy  $\delta = E_C - E_X$ , where  $E_C$  and  $E_X$  are energies of the cavity mode and of the heavy-hole exciton at zero in-plane wavevector ( $k=0$ ). The samples under study were placed into the helium-flow cryostat and kept at  $T = 3.5$  K. The photoluminescence (PL) from the pillars was collected after non-resonant excitation by a cw Ti:sapphire laser in a local minimum of the DBR reflectivity ( $\approx 110$  meV above  $E_X$ ). The laser beam was focused to a 2  $\mu\text{m}$  spot at the pillar center by a microscope objective (focal length = 4 mm, numerical aperture = 0.42). The same objective was used to collect PL. Real space images as well as the  $k$ -space images of pillars were projected on the entrance slit of a 50 cm-monochromator and after spectral dispersion were recorded by a CCD-camera. When taking real space images, the grating of the monochromator was set to the zeroth order of diffraction, and the width of the entrance slit was set to 3 mm. All experiments were performed at normal incidence of the excitation beam on the sample surface. To suppress the excitation laser light scattered from the pillar surface, a cut-off interference filter was installed in front of the entrance slit.

<sup>a)</sup>Electronic mail: kalevich@solid.ioffe.ru

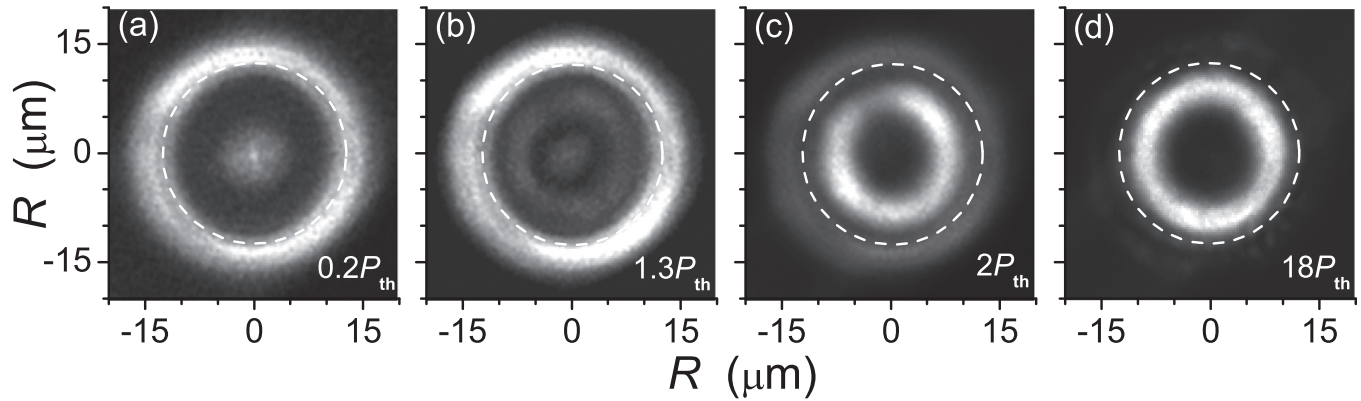


FIG. 1. Real space images of a  $25\ \mu\text{m}$  pillar measured at pumping power  $P/P_{\text{th}}=0.2$  (a),  $1.3$  (b),  $2$  (c), and  $18$  (d), where  $P_{\text{th}}=2.2$  mW. Here,  $R$  is the distance from the pillar center. White dashed circumference shows the pillar edge.  $T=3.5$  K. The brightness in each panel is normalized to its maximum over the image.

We studied pillars with the diameters of  $16$ ,  $20$ ,  $25$ ,  $30$ , and  $40\ \mu\text{m}$ . Since the main obtained results are qualitatively the same for all those pillars, we present here the data for a  $25\ \mu\text{m}$  one only.

### III. RESULTS AND DISCUSSION

Figure 1 shows real space images of a  $25\ \mu\text{m}$  pillar measured at different excitation powers. At the lowest pumping, the intensity pattern in the image is a ring with a small spot in the center (Fig. 1(a)). The inner diameter of this ring coincides with that of the pillar top shown by the dashed circumference in Fig. 1. We will show below that this “border” ring is the exciton radiation escaping from the side surface of the pillar. The central spot in Fig. 1(a) is mainly due to the scattered light of the excitation laser. With the increase of pumping intensity, the second (“inner”) ring of smaller diameter appears (Fig. 1(b)) and it becomes dominant under strong pumping, as seen in Figs. 1(c) and 1(d). According to our estimations, in the strong pumping regime ( $P/P_{\text{th}} > 3$ , where  $P_{\text{th}}=2.2$  mW is the polariton laser threshold, as will be shown below) the integrated intensity of emission of the inner ring exceeds the emission integrated over the remaining area of the pillar by two orders of magnitude. Note that the diameter of the inner ring slightly increases with the

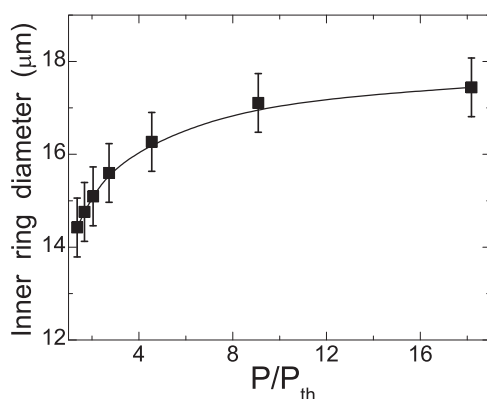


FIG. 2. Mean diameter of the inner ring as a function of excitation power. Solid line is a guide for the eye.

pump power, not exceeding the diameter of the pillar, as shown in detail in Fig. 2.

To reveal the origin of the inner and border rings, we analyzed  $k$ -space images and spatially resolved PL spectra of the pillar at different pumping intensities.

The  $k$ -space images measured by the angle-resolved PL<sup>16</sup> at low and high excitation power are shown in Figs. 3(a) and 3(b), respectively. At low pumping, the polariton dispersion exhibits a minimum at  $1.539$  eV and  $k=0$ . We observe also a broad emission line at  $1.544$  eV. It is interpreted as the PL of heavy-hole excitons escaping from the side surface of the pillar due to scattering at the imperfections of this surface, as it was already found in Ref. 5. Simulations of the polariton and exciton dispersions in the model of three coupled oscillators (not shown here) allow us to conclude that in this particular pillar the optical mode is negatively detuned from the heavy-hole exciton,  $\delta = -2$  meV. The increase of the excitation power results in an abrupt narrowing of the distribution of polariton emission over energy and angle, down to fractions of meV and a couple of angular degrees, at pump intensity exceeding the

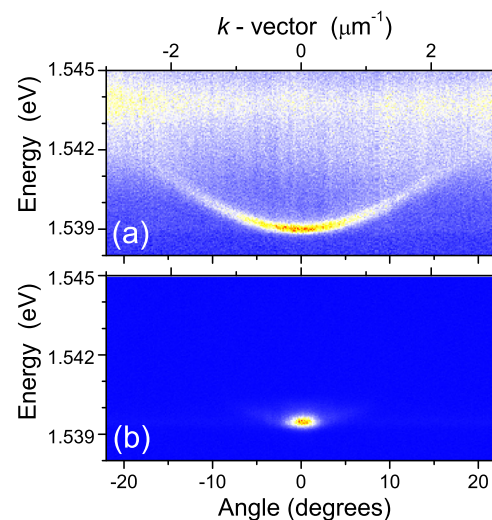


FIG. 3.  $k$ -space image of a  $25\ \mu\text{m}$  pillar normalized to its maximum brightness at (a)  $P/P_{\text{th}}=0.45$  and (b)  $P/P_{\text{th}}=4.5$ .

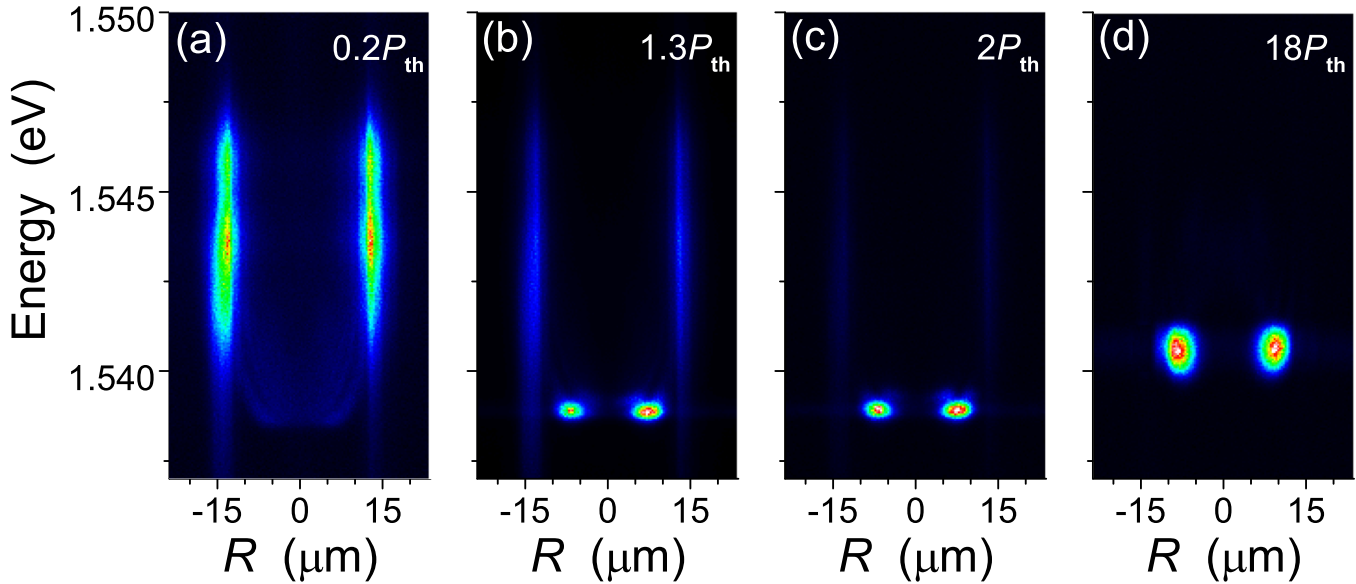


FIG. 4. Spatially and spectrally resolved emission spectra of a  $25 \mu\text{m}$  pillar at pumping power  $P/P_{\text{th}}$  equal to (a) 0.2, (b) 1.3, (c) 2, and (d) 18. The brightness in each image is normalized to its maximum.

polariton lasing threshold, as demonstrated in Fig. 3(b). This is a signature of polariton lasing, already observed in several microcavity systems under non-resonant excitation.<sup>17–19</sup>

The diameter of the real space image of the pillar on the entrance slit was about 2 mm. Using a much smaller width of the entrance slit ( $100 \mu\text{m}$ ), we could spectrally and spatially resolve the photoluminescence along the diameter of the pillar. Figure 4 shows the spectral-spatial images taken at four different excitation powers. At the lowest pumping, the spectrally broad emission from the border of the pillar dominates (Fig. 4(a)). This broad line can only be attributed to emission by heavy-hole excitons. It is peaked at 1.544 eV, which coincides with the exciton feature observed in the  $k$ -space image in Fig. 3(a), detected at the same excitation power. At smaller distances  $R$  from the pillar center, we also observe a weak polariton emission at lower energies. The edge of this emission spectrum at 1.539 eV is well below the exciton resonance and coincides with the bottom of the low polariton branch in Fig. 3(a).

The polariton emission from the inner part of the pillar increases with the pumping power. At  $P \approx P_{\text{th}}$ , it starts concentrating in two small spots at  $|R| \approx 7 \mu\text{m}$  and the energy of 1.539 eV, as shown in Fig. 4(b). Under further increase of pumping, these two localized spots of polariton emission become dominating over the incoherent exciton emission (Figs. 4(c) and 4(d)). The distance between these spots coincides with the inner ring diameter in Fig. 1, thereby indicating that these spots originate from the inner ring radiation. Figure 5(a) shows the peak intensity of the PL from one of these spots and the peak intensity of the border emission as functions of the pumping intensity. The border PL intensity linearly increases with the pumping intensity (triangles in Fig. 5(a)), that confirms its excitonic origin. On the contrary, the inner-ring emission (polariton emission) increases super-linearly (squares in Fig. 5(a)): it increases by two orders of magnitude with the pumping power changing by only a factor of 2, from  $P = P_{\text{th}}$  to  $P = 2P_{\text{th}}$ . The superlinear increase

of polariton emission at  $P_{\text{th}} \leq P \leq 2P_{\text{th}}$  is characteristic of the formation of a polariton condensate by stimulated scattering. The condensate formation is also confirmed by a strong spectral (squares in Fig. 5(b)) and angular (Fig. 5(c)) narrowing of the polariton emission with the pumping power increase up to  $P \approx 2P_{\text{th}}$ . A sharp, down to  $2^\circ$ , narrowing of the angular distribution of the polariton emission at  $P \gg P_{\text{th}}$  means that the light beam emitted by the polariton laser has the shape of a tube directed along the pillar axis.

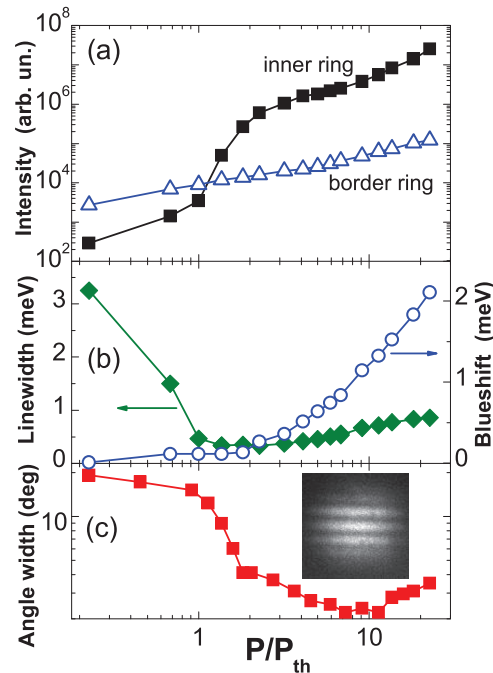


FIG. 5. (a) Emission intensity of polaritons (squares) and of excitons (triangles). (b) Spectral linewidth (diamonds) and blueshift (circles) of polariton emission. (c) Full width at half-maximum of the angular distribution of polariton emission.  $T = 3.5 \text{ K}$ . Inset in panel (c): fringe pattern emerging when light beams from two spots from the opposite sides of the ring (see Fig. 4) are superimposed at  $P/P_{\text{th}} = 6$ .

Formation of the polariton condensate in the shape of a ring, whose diameter greatly exceeds the size of the excitation spot, is caused, in our opinion, by interaction of the polaritons with the exciton cloud formed from electron-hole pairs created by the nonresonant pump in the pillar center. Because of a slow loss of energy by excitons via emission of acoustic phonons, and of a long exciton lifetime (a considerable part of excitons under nonresonant pumping forms outside the light cone and cannot recombine radiatively), a large population of excitons builds up. Since excitons have short diffusion length,<sup>20</sup> they accumulate in the vicinity of the excitation spot. Their repulsive exchange interaction with polaritons creates for the latter a potential hill in the center of the pillar.<sup>13</sup> Together with the infinitely high potential barrier at the pillar border, this results in the formation of a localizing potential having the shape of a circular groove, which serves as a trap facilitating polariton condensation. With increase of the pump power and, therefore, of the concentration of excitons, the potential near the excitation spot rises, and the diameter of the condensate ring should become somewhat larger. Indeed, as seen in Fig. 2, the ring diameter increases from 14.4 to 17.5  $\mu\text{m}$  with the growth of  $P$  from  $1.3P_{\text{th}}$  to  $18P_{\text{th}}$ . The inner ring diameter up to 30  $\mu\text{m}$  was observed in the 40  $\mu\text{m}$  pillar.

This result can be compared with the observation by Christmann *et al.*<sup>12</sup> on a planar cavity. They have observed a radially symmetric condensate of polaritons, accelerating outwards from the excitation spot, with a dark circle in the center. The size of the condensate was much larger than the radius of the central dark circle, and it did not have a pronounced outer boundary. In our case, the outer boundary of the condensate is defined by the pillar edge, which is why it takes the shape of a high-contrast, thin ring.

The polariton emission in Fig. 4 demonstrates a blue shift, as shown in detail in Fig. 5(b) (circles). The blue shift may originate either from the polariton interaction with excitons or from polariton-polariton repulsion within the condensate. When, as in our case, the pillar diameter is much larger than the size of the excitation spot, localization regions of the polariton condensate and of the exciton reservoir are spatially separated. In this case, the blue shift weakly depends on the exciton-polariton interaction and is mainly determined by the polariton-polariton interaction in the condensate.<sup>13</sup>

In this paper, we concentrated on the lowest energy polariton state, which provides the strongest emission intensity. Weaker emission of polaritons with higher energies, seen in Fig. 4, will be considered elsewhere.

The inset in Fig. 5(c) presents the Young interferometry image measured, by superimposing the light beams emitted by two spots shown in Fig. 4, at  $P/P_{\text{th}} = 6$ . A clear fringe pattern is observed beyond the polariton lasing threshold, while it is absent at  $P < P_{\text{th}}$ . Since these two spots in Fig. 4 are situated at the opposite ends of the ring diameter (the arc length between the spots is about 26  $\mu\text{m}$ ), this observation confirms the buildup of a spatial coherence in the whole ring polariton condensate.

## IV. CONCLUSION

To conclude, a ring-shaped polariton condensate is formed in a cylindrical-pillar microcavity under non-resonant optical pumping at the center of the pillar. The diameter of the ring is much larger than the excitation spot and may be controlled by the pumping intensity.

## ACKNOWLEDGMENTS

This work was partly supported by the Russian Ministry of Education and Science (Contract No. 11.G34.31.0067). P.G.S. and S.I.T. acknowledge support from the Russian exchange grant EU FP7 IRSES “POLATER” and P.G.S. is indebted to Greek GSRT program “ARISTEIA” (1978) and FP7 ITN “INDEX” (289968) projects for financial support.

- <sup>1</sup>A. Imamoğlu, R. J. Ram, S. Pau, and Y. Yamamoto, *Phys. Rev. A* **53**, 4250 (1996).
- <sup>2</sup>S. Christopoulos, G. Baldassarri Höger von Högersthal, A. J. D. Grundy, P. G. Lagoudakis, A. V. Kavokin, J. J. Baumberg, G. Christmann, R. Butté, E. Feltn, J.-F. Carlin, and N. Grandjean, *Phys. Rev. Lett.* **98**, 126405 (2007).
- <sup>3</sup>C. Schneider, A. Rahimi-Iman, N. Y. Kim, J. Fischer, I. G. Savenko, M. Amthor, M. Lermer, A. Wolf, L. Worschech, V. D. Kulakovskii, I. A. Shelykh, M. Kamp, S. Reitzenstein, A. Forchel, Y. Yamamoto, and S. Höfling, *Nature* **497**, 348 (2013).
- <sup>4</sup>P. Bhattacharya, B. Xiao, A. Das, S. Bhowmick, and J. Heo, *Phys. Rev. Lett.* **110**, 206403 (2013).
- <sup>5</sup>D. Bajoni, P. Senellart, E. Wertz, I. Sagnes, A. Miard, A. Lemaître, and J. Bloch, *Phys. Rev. Lett.* **100**, 047401 (2008).
- <sup>6</sup>M. Maragkou, A. J. D. Grundy, E. Wertz, A. Lemaître, I. Sagnes, P. Senellart, J. Bloch, and P. G. Lagoudakis, *Phys. Rev. B* **81**, 081307(R) (2010).
- <sup>7</sup>F. Tassone and Y. Yamamoto, *Phys. Rev. B* **59**, 10830 (1999).
- <sup>8</sup>C. Ciuti, P. Schwendimann, B. Deveaud, and A. Quattropani, *Phys. Rev. B* **62**, R4825 (2000).
- <sup>9</sup>M. Vladimirova, S. Cronenberger, D. Scalbert, K. V. Kavokin, A. Miard, A. Lemaître, J. Bloch, D. Solnyshkov, G. Malpuech, and A. V. Kavokin, *Phys. Rev. B* **82**, 075301 (2010).
- <sup>10</sup>M. Wouters, I. Carusotto, and C. Ciuti, *Phys. Rev. B* **77**, 115340 (2008).
- <sup>11</sup>A. Askitopoulos, H. Ohadi, A. V. Kavokin, Z. Hatzopoulos, P. G. Savvidis, and P. G. Lagoudakis, *Phys. Rev. B* **88**, 041308(R) (2013).
- <sup>12</sup>G. Christmann, G. Tosi, N. G. Berloff, P. Tsotsis, P. S. Eldridge, Z. Hatzopoulos, P. G. Savvidis, and J. J. Baumberg, *Phys. Rev. B* **85**, 235303 (2012).
- <sup>13</sup>L. Ferrier, E. Wertz, R. Johne, D. D. Solnyshkov, P. Senellart, I. Sagnes, A. Lemaître, G. Malpuech, and J. Bloch, *Phys. Rev. Lett.* **106**, 126401 (2011).
- <sup>14</sup>E. Wertz, L. Ferrier, D. D. Solnyshkov, R. Johne, D. Sanvitto, A. Lemaître, I. Sagnes, R. Grousson, A. V. Kavokin, P. Senellart, G. Malpuech, and J. Bloch, *Nature Phys.* **6**, 860 (2010).
- <sup>15</sup>P. Tsotsis, P. S. Eldridge, T. Gao, S. I. Tsintzos, Z. Hatzopoulos, and P. G. Sawidis, *New J. Phys.* **14**, 023060 (2012).
- <sup>16</sup>R. Houdré, C. Weisbuch, R. P. Stanley, U. Oesterle, P. Pellandini, and M. Illegems, *Phys. Rev. Lett.* **73**, 2043 (1994).
- <sup>17</sup>H. Deng, G. Weihs, C. Santori, J. Bloch, and Y. Yamamoto, *Science* **298**, 199 (2002).
- <sup>18</sup>J. Kasprzak, M. Richard, S. Kundermann, A. Baas, P. Jeambrun, J. M. J. Keeling, F. M. Marchetti, M. H. Szymańska, R. André, J. L. Staehli, V. Savona, P. B. Littlewood, B. Deveaud, and L. S. Dang, *Nature* **443**, 409 (2006).
- <sup>19</sup>R. Balili, V. Hartwell, D. Snoke, L. Pfeiffer, and K. West, *Science* **316**, 1007 (2007).
- <sup>20</sup>W. Heller, A. Filoramo, P. Roussignol, and U. Bockelmann, *Solid-State Electron.* **40**, 725 (1996).